
Fully Convolutional Pixel Adaptive Image Denoiser

Sungmin Cha and Taesup Moon

Department of Electrical and Computer Engineering
Sungkyunkwan University
Suwon, Korea 16419
{csm9493, tsmoon}@skku.edu

Abstract

We propose a new denoising algorithm, dubbed as Fully Convolutional Adaptive Image Denoiser (FC-AIDE), that can learn from offline supervised training set with a fully convolutional neural network architecture as well as adaptively fine-tune the denoiser for each given noisy image. We mainly follow the framework of the recently proposed Neural AIDE, which formulates the denoiser to be context-based pixelwise affine mappings and utilizes the unbiased estimator of MSE of such denoisers. The three main contributions we make to significantly improve upon the original Neural AIDE are the followings; 1) implementing a novel fully convolutional architecture that boosts the base supervised model, 2) introducing data augmentation for adaptive fine-tuning to achieve much stronger adaptivity, and 3) proposing an effective unknown noise level estimation method. As a result, FC-AIDE is shown to significantly outperform the state-of-the-art CNN-based denoisers on two standard benchmark dataset as well as on a much challenging blind denoising dataset, in which nothing is known about the noise level, noise distribution, or image characteristics.

1 Introduction

Image denoising, which tries to recover a clean image from its noisy observation, is one of the oldest and most prevalent problems in image processing and low-level computer vision. While numerous algorithms have been proposed over the past few decades, *e.g.*, [7, 3, 6, 11, 8, 13], the current throne-holders in terms of the average denoising performance are convolutional neural network (CNN)-based methods [26, 14, 22, 2].

The main idea behind the CNN-based method is to treat denoising problem as a supervised regression problem; namely, first collect numerous clean-noisy image pairs as a supervised training set, then learn a regression function that maps the noisy image to the clean image. Such approach is relatively simple since it does not require to assume any complex priors on the underlying clean images and let CNN figure out to learn the correct mapping for the noisy images in the vast training data. Despite the conceptual simplicity, several recent variations of the CNN-based denoisers using residual learning [26], skip-connections [14], and DenseNet-like structure [22] have achieved impressive state-of-the-art denoising performances.

However, we stress that one apparent drawback exists in above methods; they are solely based on offline batch training of CNN, hence, lack adaptivity to the given noisy image subject to denoising. Such absence of adaptivity, which is typically possessed in other prior or optimization-based methods, *e.g.*, [7, 3, 6, 11, 8, 13], can seriously deteriorate the denoising performance of the CNN-based methods in multiple practical scenarios in which various mismatches exist between the training data and the given noisy image. One category of such mismatch is the noise mismatch, in which the noise level or the distribution for the given noisy image is different from what the CNN has been trained for. For example, if the given image is corrupted by Laplacian noise with $\sigma = 50$, the CNN-based

denoiser trained for Gaussian noise with $\sigma = 25$ will perform poorly. The other category is the image mismatch, in which the image characteristics of the given noisy image are not well represented in the training set for CNN. For example, when the given noisy image is a medical image (*e.g.*, X-ray or MRI) while CNN is trained with natural images, or when the given image has a specific regular textures with high self-similarity that cannot be found in the training set, the CNN-based denoisers will again suffer from low accuracy. Although the so-called blind training, which was proposed in [26] for noise level mismatch, can partially address some of the above problems by building a composite training set with multiple noise and image characteristics, the limitation is clear as one cannot contain all the variations sufficiently in the training set beforehand.

To that end, we propose a new denoising algorithm that can learn from offline supervised training set with a fully convolutional architecture, like other CNN-based denoisers, as well as adaptively fine-tune the denoiser for each given noisy image, like other prior or optimization based methods. The main vehicle for devising our algorithm, dubbed as FC-AIDE (Fully Convolutional Adaptive Image Denoiser), is the framework recently proposed in [4]. Namely, we formulate our denoiser to be context-based pixelwise affine mappings and exploit the independence of the noise to obtain the SURE (Stein’s Unbiased Risk Estimator)[21]-like estimated losses of the mean-squared errors (MSE) for the affine mappings. Then, the mapping coefficients for each pixel are learned with a fully convolutional neural network first by *supervised training* on a offline training set via minimizing the mean-squared error (MSE), then by *adaptively fine-tuning* the network with the given noisy image via minimizing the devised estimated losses. Following this framework, we significantly improve the original Neural AIDE [4] by making the following three contributions. Firstly, we devise a novel fully convolutional architecture instead of the simple fully-connected structure in [4] so that the performance of the base supervised model can be boosted. Secondly, we utilize data augmentation for regularizing the fine-tuning step and adaptively learn the pixelwise affine mappings tailored for the given noisy image to achieve larger and more robust improvements. Thirdly, we propose a novel noise level (*i.e.*, the standard deviation σ) estimation algorithm based on the characteristic of our devised estimated loss function. The resulting estimated σ is then used for a challenging blind denoising setting, in which nothing is known about the noise σ , noise distribution, nor image characteristics.

With above three contributions, we show our FC-AIDE outperforms all previous state-of-the-art denoising methods on two standard benchmark datasets. Moreover, the adaptive fine-tuning is shown to be especially powerful when various mismatch cases exist. For example, in the blind denoising setting mentioned above, our blindly trained FC-AIDE adaptively fine-tuned with the estimated σ for each image is shown to significantly outperform the blindly trained model in [26], DnCNN-B, for more than 2dB in PSNR. Furthermore, FC-AIDE can denoise the images with strong self-similarities as well as the non-local filter (NLF) based methods, *e.g.*, BM3D [6], whereas other CNN-based denoisers are well-known to perform poorly on those images.

Related Work. Our method is following the universal denoising framework first proposed in [25], which in fact inspired the classic non-local means algorithm [3]. Namely, in order to achieve the adaptivity, we do not assume any priors or probabilistic assumptions on the clean image, but maintain the *semi-stochastic setting* as in [25], *i.e.*, only treat the noise as random variables and denoise based on the information aggregated from noisy contexts. Extending the original *discrete* denoising framework of [25] to grayscale image denoising have also been considered in [17, 20] by doing some clever context quantization and aggregation, but the denoising performance was not very satisfactory. The SURE-based estimators are also widely used, *e.g.*, [7, 9], but they typically select a few tunable hyperparameters via minimizing the unbiased estimates of MSE. In contrast, using the unbiased estimate as an empirical risk in the empirical risk minimization (ERM) framework to learn the entire parametric model (*e.g.*, neural network) was first proposed in [16, 4]. Such method can be also interpreted as neural networks carrying out implicit context aggregation for denoising.

2 Problem Setting and Preliminaries

We generally follow [4] but introduce more compact notations. First, we denote $\mathbf{x} \in \mathbb{R}^n$ as the clean image and $\mathbf{Z} \in \mathbb{R}^n$ as its noise-corrupted version. We assume $\mathbf{Z} = \mathbf{x} + \mathbf{N}$, in which $\mathbb{E}(\mathbf{N}) = \mathbf{0}$ and $\text{Cov}(\mathbf{N}) = \sigma^2 \mathbf{I}_{n \times n}$. Note we do *not* necessarily assume \mathbf{N} is Gaussian. Moreover, we treat the clean \mathbf{x} as an *individual* image without any prior or probabilistic model and only treat the noisy image \mathbf{Z} as random, which is reflected in the upper case notation.

A denoiser is generally denoted as $\hat{\mathbf{X}}(\mathbf{Z}) \in \mathbb{R}^n$, of which the i -th reconstruction, $\hat{X}_i(\mathbf{Z})$, is a function of the entire noisy image \mathbf{Z} . The standard loss function to measure the denoising quality is MSE denotes as $\Lambda_n(\mathbf{x}, \hat{\mathbf{X}}(\mathbf{Z})) \triangleq \frac{1}{n} \|\mathbf{x} - \hat{\mathbf{X}}(\mathbf{Z})\|_2^2$. Conventionally, the MSE is compared in the dB-scale using the Peak Signal-to-Noise-Ratio (PSNR) defined as $10 \log_{10}(255^2 / \Lambda_n(\mathbf{x}, \hat{\mathbf{X}}(\mathbf{Z})))$.

While $\hat{X}_i(\mathbf{Z})$ can be any general function, [4] considers a specific affine function form for the denoiser, i.e., $\hat{X}_i(\mathbf{Z}) = a(\mathbf{Z}^{-i}) \cdot Z_i + b(\mathbf{Z}^{-i})$, in which \mathbf{Z}^{-i} stands for the entire noisy image *except* for the i -th pixel, Z_i . Note $\hat{X}_i(\mathbf{Z})$ can be a highly nonlinear function of \mathbf{Z} as $a(\cdot)$ and $b(\cdot)$ can be any nonlinear functions. For such a denoiser, [4] defines an unbiased estimated loss function of MSE,

$$\mathbf{L}_n(\mathbf{Z}, \hat{\mathbf{X}}(\mathbf{Z}); \sigma^2) \triangleq \frac{1}{n} \|\mathbf{Z} - \hat{\mathbf{X}}(\mathbf{Z})\|_2^2 + \frac{\sigma^2}{n} \sum_{i=1}^n [2a(\mathbf{Z}^{-i}) - 1]. \quad (1)$$

Note (1) does *not* depend on \mathbf{x} , and the following lemma states the unbiasedness of (1).

Lemma 1 *For any additive noise \mathbf{N} with $\mathbb{E}(\mathbf{N}) = 0$, $\text{Cov}(\mathbf{N}) = \sigma^2 \mathbf{I}$, we have*

$$\mathbb{E} \mathbf{L}_n(\mathbf{Z}, \hat{\mathbf{X}}(\mathbf{Z}); \sigma^2) = \mathbb{E} \Lambda_n(\mathbf{x}, \hat{\mathbf{X}}(\mathbf{Z})) \quad (2)$$

for $\hat{\mathbf{X}}(\mathbf{Z})$ that has the form as mentioned above. Moreover, when \mathbf{N} is white Gaussian (i.e., AWGN), then, $\mathbf{L}_n(\mathbf{Z}, \hat{\mathbf{X}}(\mathbf{Z}); \sigma^2)$ coincides with the Stein's Unbiased Risk Estimate (SURE)[21].

Remark: The proof of the lemma is given in the Supplementary Material. Note the unbiasedness in (5) holds for *any* additive white noise, not necessarily only for Gaussian. Such property enables the strong adaptivity of our algorithm that we show in the later sections.

Neural AIDE [4], denoted as $\hat{\mathbf{X}}_{\text{N-AIDE}}(\mathbf{w}, \mathbf{C}_{k \times k}) = \{\hat{X}_i(\mathbf{w}, \mathbf{C}_{i, k \times k})\}$, is a neural network-based denoiser that reconstructs the i -th pixel as

$$\hat{X}_i(\mathbf{w}, \mathbf{C}_{i, k \times k}) = a(\mathbf{w}, \mathbf{C}_{k \times k}^{-i}) \cdot Z_i + b(\mathbf{w}, \mathbf{C}_{k \times k}^{-i}), \quad (3)$$

in which $\mathbf{C}_{i, k \times k}$ stands for the two-dimensional (2-D) noisy $k \times k$ patch (or context) surrounding Z_i , $\mathbf{C}_{k \times k}^{-i}$ is the same as $\mathbf{C}_{i, k \times k}$ but *without* Z_i , and $a(\mathbf{w}, \mathbf{C}_{k \times k}^{-i})$ and $b(\mathbf{w}, \mathbf{C}_{k \times k}^{-i})$ are the two scalar outputs of a fully-connected neural network with parameter \mathbf{w} that takes $\mathbf{C}_{k \times k}^{-i}$ as an input. Note that \mathbf{w} does not depend on location i , hence, the denoising by Neural AIDE is done in a sliding-window fashion; that is, the neural network subsequently takes $\mathbf{C}_{k \times k}^{-i}$ as an input and generates the affine mapping coefficients for Z_i to obtain the reconstruction for pixel i .

As mentioned in the Introduction, the training of the network parameter \mathbf{w} is done in two stages. Firstly, for *supervised training*, a training set $\mathcal{D} = \{(\tilde{x}_i, \tilde{\mathbf{C}}_{i, k \times k})\}_{i=1}^N$ based on many clean-noisy image pairs is first collected, and a supervised model, $\tilde{\mathbf{w}}$, is learned by minimizing the MSE on \mathcal{D} , $\Lambda_N(\tilde{\mathbf{x}}, \tilde{\mathbf{X}}(\mathbf{w}, \tilde{\mathbf{C}}_{k \times k}))$. Secondly, for a given noisy image \mathbf{Z} subject to denoising, *adaptive fine-tuning* of the supervised model $\tilde{\mathbf{w}}$ is carried out by further minimizing the estimated loss $\mathbf{L}_n(\mathbf{Z}, \hat{\mathbf{X}}(\mathbf{w}, \mathbf{C}_{k \times k}); \sigma^2)$ starting from $\tilde{\mathbf{w}}$. The fine-tuned model $\hat{\mathbf{w}}$ is then used to obtain the affine mapping for each pixel i as in (3), and \mathbf{Z} is pixelwise denoised with those mappings.

3 Fully Convolutional Pixel Adaptive Image Denoiser (FC-AIDE)

3.1 Fully convolutional QED architecture

While the performance of Neural AIDE in [4] was encouraging, the final denoising performance was slightly worse (about $\sim 0.15\text{dB}$) than the CNN-based state-of-the-art, DnCNN-S [26]. We believe such performance difference is primarily due to the simple fully-connected architecture used in [4, Figure 1] as opposed to the fully convolutional architectures in recent work, e.g., [26, 14, 22].

In order to utilize the convolutional architecture for our model, we first make an observation that the sliding-window denoising of the original Neural AIDE is indeed a convolution operation. That is, once we use masked $k \times k$ convolution filters (i.e., the center set to 0) for the first layer and use ordinary 1×1 filters for the higher layers, the resulting fully convolutional network operating

on a noisy image becomes equivalent to the fully-connected network in [4, Figure 1] working in a sliding-window fashion. Note when standard zero-padding is used, the output of the network has the same size as the input image since no pooling is used, and it consists of two channels, one for $a(\mathbf{w}, \mathbf{C}_{k \times k}^{-i})$ and the other for $b(\mathbf{w}, \mathbf{C}_{k \times k}^{-i})$ in (3).

From above observation, we identify a critical constraint for implementing a fully convolutional architecture for the denoisers that have the form (3); namely, for *any* feature maps at *any* layer, the value at the i -th location should *not* depend on Z_i , and the filters at the output layer should keep the 1×1 structure. The reason for this constraint is to maintain the independence between $(a(\mathbf{w}, \mathbf{C}_{k \times k}^{-i}), b(\mathbf{w}, \mathbf{C}_{k \times k}^{-i}))$ and Z_i given the underlying clean image \mathbf{x} , since such conditional independence is the key for the unbiasedness of $\mathbf{L}_n(\mathbf{Z}, \hat{\mathbf{X}}(\mathbf{w}, \mathbf{C}_{k \times k}); \sigma^2)$ shown in Lemma 2. From this constraint, we can easily see that simply stacking ordinary convolution filters of size larger than 1×1 in the second and higher layers is not feasible for designing our denoiser. Thus, for the naive convolutional implementation mentioned above, the only way to increase the patch size (or the receptive field) is to use larger filter in the first layer while fixing the rest to 1×1 , but, such structure may not realize the full potential of CNN in learning a good denoising function. In fact, the performance of Neural AIDE does not improve beyond $k = 17$, whereas DnCNN-S uses the receptive field of 35 by stacking 17 layers of 3×3 filters.

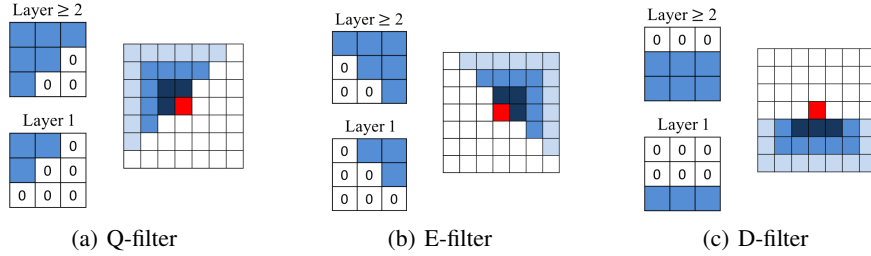


Figure 1: QED filters and the receptive field for the red pixel at Layer 3 for each filter class.

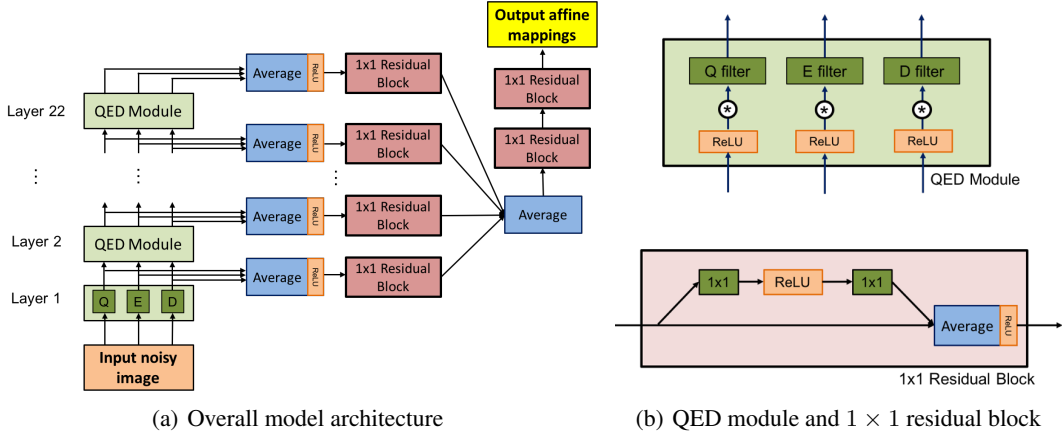


Figure 2: Fully convolutional model architecture of FC-AIDE

We note a similar constraint as above has also appeared in [23], in which utilizing the “one-sided” contexts to generate feature maps of CNN was considered for sequentially generating image pixels. In contrast, in our denoising model, (3), we need to utilize the whole “double-sided” context, $\mathbf{C}_{k \times k}^{-i}$, to generate a feature map for location i such that the two affine mapping coefficients can be obtained from the feature map. To that end, we propose three different convolution filter classes, dubbed as QED filters, in order to gradually increase the receptive field with the deep CNN architecture beyond 1×1 structure, while satisfying the conditional independence constraint. Figure 1(a)~(c) depict the masked 3×3 convolution filters applied for each layer of the Q-, E-, and D-filter classes, respectively. Moreover, the figures also show the receptive fields (colored in blue) associated with each filter class,

for the red pixel in the Layer 3 feature map. From the figures, we can see that once the input image is processed by each filter class separately, combining the three types of feature maps at layer ℓ (e.g., averaging) generates a feature map of which the i -th pixel depends on $\mathbf{C}_{k \times k}^{-i}$ with $k = 2\ell + 1$ and satisfies the constraint.

Figure 2(a) shows the overall model architecture of our FC-AIDE, $\hat{\mathbf{X}}_{\text{FC-AIDE}}(\mathbf{w}, \mathbf{C}_{k \times k})$, that utilizes above described QED filters. Namely, the QED modules, which apply each filter class separately on its own input feature map as shown in Figure 2(b), are stacked up to 22 layers, and each layer combines the output feature maps (before ReLU) from the three filter classes via averaging. The combined feature map from each layer then goes through a residual block with two 1×1 filters shown in Figure 2(b), after which the feature maps from all layers (with different receptive fields) are combined again via averaging. The resulting combined feature maps finally go through another two residual blocks, followed by the final 1×1 output layer. In Section 4, we show the new FC-AIDE can significantly outperform the original Neural AIDE as well as other CNN-based state-of-the-arts.

3.2 Data augmentation for fine-tuning

The fully-convolutional architecture in Section 3.1 basically expands the function approximation capability and improves the base supervised model benefitting from the abundant training data. For the adaptive fine-tuning, however, the only “training data” is the given noisy image \mathbf{Z} , which may cause the over-fitting; *i.e.*, the estimated loss $\mathbf{L}_n(\cdot)$ may be minimized, but the true MSE $\mathbf{A}_n(\cdot)$ may not be minimized as much.

In order to address such data-scarcity issue, we utilize data augmentation as a regularization method for the fine-tuning step. Namely, we denote \mathbf{Z}_h , \mathbf{Z}_v , and \mathbf{Z}_{hv} as images that are flipped horizontally, vertically, and both horizontally and vertically, respectively. Then, we fine-tune the supervised model $\hat{\mathbf{w}}$ by minimizing the sum of the estimated losses on all four images including the original image \mathbf{Z}_o :

$$\sum_{j=\{o,h,v,hv\}} \mathbf{L}_n(\mathbf{Z}_j, \hat{\mathbf{X}}(\mathbf{w}, \mathbf{C}_{k \times k}^j); \sigma^2), \quad (4)$$

in which $\mathbf{C}_{k \times k}^j$ stands for the $k \times k$ patches from the image \mathbf{Z}_j . Once the fine-tuning is done, the final denoising result is then obtained by averaging the denoising results obtained from applying $\hat{\mathbf{X}}_{\text{FC-AIDE}}(\hat{\mathbf{w}}, \mathbf{C}_{k \times k})$ to the 4 images, \mathbf{Z}_o , \mathbf{Z}_h , \mathbf{Z}_v , and \mathbf{Z}_{hv} , separately. We show in Section 4 that such simple data augmentation makes the adaptive fine-tuning more powerful in enlarging the performance improvement over the supervised model and attaining strong adaptivity to address the various mismatch issues described in the Introduction.

3.3 Estimating unknown noise standard deviation

One main assumption for the two improvements in Section 3.1 and 3.2 is that the noise σ is *known*. Namely, σ should be known for generating the noisy images in the supervised training set as well as for computing (4) for the adaptive fine-tuning. While such assumption is common in most denoising algorithms, a mismatch between the assumed σ and the true σ can seriously degrade the denoising performance.

As a remedy for such noise level mismatch, [26] proposed the blindly trained model, DnCNN-B, which trains the network with multiple levels of σ randomly selected from a certain range, *e.g.*, $[0, 50]$. It was shown in [26] that DnCNN-B is quite robust to the noise uncertainty, and our FC-AIDE can be also blindly trained during the supervised training phase in a similar manner. Going one step further, we propose an unknown σ estimation method so that the estimated $\hat{\sigma}$ can be used for fine-tuning to further improve the performance of the blindly trained supervised model.

The main gist of our σ estimation method follows from the observation that the estimated loss function, (1), consists of two terms; one with the ℓ_2 -norm and the other associated with σ^2 . We can easily see that if there were no second term, the network will try to output $a(\mathbf{Z}^{-i}) \approx 1$ and $b(\mathbf{Z}^{-i}) \approx 0$ for all i when minimizing (1). However, due to the second term, $a(\mathbf{Z}^{-i})$'s should shrink to make the overall sum small, and σ^2 is acting like a regularization parameter in the common penalty-based regularization methods. In fact, when $\frac{1}{n} \sum_{i=1}^n a(\mathbf{Z}^{-i}) < \frac{1}{2}$, the second term can even be made negative, and the fine-tuning step essentially tries to find the right trade-off between the two terms by controlling $a(\mathbf{Z}^{-i})$'s and $b(\mathbf{Z}^{-i})$'s. Now, suppose we use $\hat{\sigma}$ that is larger than the

true σ for computing (1). Then, since the effect of the second term increases, we see that $a(\mathbf{Z}^{-i})$'s will prefer to shrink further than using the correct σ . Moreover, when $\tilde{\sigma}$ is significantly larger than σ , one can expect that the overall value of (1) can become negative after fine-tuning. We can see this by considering a simple case of constant clean image, *e.g.*, $\mathbf{x} = 0$. In such case, $\mathbf{Z} = \mathbf{N}$, and $a(\mathbf{Z}^{-i}) = 0$, $b(\mathbf{Z}^{-i}) = \mathbb{E}(Z_i) = 0$ makes the first term become σ^2 and the second term become $-\tilde{\sigma}^2$. On the contrary, when $\tilde{\sigma}$ is smaller than σ , the effect of the second term decreases as the shrinkage of $a(\mathbf{Z}^{-i})$ may not be as much as using the true σ . Thus, in this case, (1) may not tend to fall beyond 0 as the ℓ_2 -norm term can become sufficiently small with relatively larger $a(\mathbf{Z}^{-i})$.

Based on this observation, we propose a simple binary search algorithm to estimate unknown σ among $\Sigma = \{5, 10, \dots, 95, 100\}$, by iteratively carrying out fine-tuning of a randomly initialized FC-AIDE with different σ 's and checking whether the estimated loss becomes negative or not. In Supplementary Material, we present an example that empirically confirms our above observation and give formal definition of the binary search algorithm. The resulting estimated $\hat{\sigma}$ is then used to fine-tune the blindly trained FC-AIDE model to further improve the denoising performance. Our experimental results on a challenging blind denoising set show such σ estimation is very accurate and leads to impressive performance boost of the blindly trained model.

4 Experimental results

4.1 Data and experimental setup

Training details. For the supervised training, we collected 3000 publicly available images, out of which 300 were taken from train/validation sets in the Berkeley Segmentation Dataset (BSD) [15] and the remaining 2700 were taken from Pascal VOC 2012 Dataset [10]. From each image, we cropped $128 \times 50 \times 50$ patches to obtain 128×3000 overall patches. We used noise augmentation for generating every mini-batch of clean-noisy patch pair for training of both σ -specific models and blind model. We used 64 filters for all QED filters at all layers, and 128 filters for the 1×1 filters in the residual block. Learning rates of 0.001 and 0.0001 were used for supervised training and fine-tuning, respectively, and Adam [12] optimizer was used. Learning rate decay was used only for the supervised training, and dropout or Batch-Norm were not used. All our experiments used Keras with Tensorflow backend and NVIDIA GeForce GTX1080TI with CUDA 8.0.

Evaluation data. We first used two benchmark datasets, Set13 and BSD68 [19], to objectively compare our algorithm with other methods for Gaussian denoising. Five different noise levels, $\sigma = \{15, 25, 30, 50, 75\}$, were tested. In Set13, we additionally included 3 images with very different textures, {Flinstone, Einstein, Shannon}, to the standard 10 benchmark natural images. All the images in Set13 are visualized in the Supplementary Material. BSD68 consists of 68 natural grayscale images. Furthermore, we generated three additional datasets to evaluate and compare the adaptivities of the algorithms. BSD/Laplacian is the BSD68 images corrupted by Laplacian noise with $\sigma = 30$, and Medical/Gaussian is a set of 60 medical images (20 images each from the CT, MRI, and X-ray modalities) corrupted by Gaussian noise with $\sigma = 30$. The medical images were downloaded from the open repositories [24, 1, 5] and the sizes were made to 400×400 . Samples of the medical images are also given in the Supplementary Material. The former is generated for the noise distribution mismatch case, and the latter is for the image characteristics mismatch case as the training data for CNN-based denoisers, including FC-AIDE, are natural images with Gaussian noise. Finally, we also generated Blind Denoising Set, which consists of mixture of natural and medical images corrupted by Gaussian or Laplacian noise with various σ levels. That is, for each noise distribution, we randomly sampled 30 images from BSD68 and 10 images from each of the CT/MRI/X-ray modalities, then corrupted each image with randomly selected σ in $\{15, 25, 50, 75\}$. Thus, there are total 120 images in the set, and the sizes of the images were set to 400×400 .

Table 1: PSNR(dB) on Set13.

σ	BM3D	RED	MemNet	DnCNN-S	DnCNN-B	N-AID _S	N-AID _S +FT	FC-AID _S	FC-AID _S +FT	FC-AID _B	FC-AID _B +FT
15	31.98	-	-	32.21	31.58	31.77	32.30	32.08	32.59	31.72	32.52
25	29.44	-	-	29.63	29.22	28.64	29.67	29.57	30.14	29.34	30.03
30	28.56	28.91	28.83	28.64	28.41	-	-	28.73	29.28	28.50	29.19
50	26.05	26.28	26.39	26.09	26.07	25.73	26.35	26.24	26.87	26.05	26.77
75	24.16	-	-	24.03	18.33	23.64	24.31	24.24	24.97	21.07	24.89

Table 2: PSNR(dB) on BSD68.

σ	BM3D	RED	MemNet	DnCNN-S	DnCNN-B	N-AID _S	N-AID _{S+FT}	FC-AID _S	FC-AID _{S+FT}	FC-AID _B	FC-AID _{B+FT}
15	31.07	-	-	31.72	31.60	31.47	31.58	31.63	31.75	31.47	31.72
25	28.56	-	-	29.22	29.15	28.95	29.06	29.18	29.31	29.04	29.26
30	27.74	28.45	28.42	28.35	28.34	-	-	28.35	28.49	28.24	28.44
50	25.60	26.29	26.34	26.21	26.20	25.91	26.04	26.24	26.38	26.12	26.33
75	24.19	-	-	24.62	18.68	24.30	24.47	24.74	24.87	21.42	24.76

The baseline methods that we mainly compared are BM3D [6], RED [14], MemNet [22], DnCNN-S and DnCNN-B [26], and N-AID_S and N-AID_{S+FT} [4]. For RED, MemNet, DnCNN and Neural AIDE, we downloaded the models from the authors’ website and carried out the denoising in our evaluation dataset. Moreover, we note RED, MemNet, DnCNN-S, and N-AID_S are the supervised-only models, DnCNN-B is the blindly trained model with σ range of $[0, 55]$, and N-AID_{S+FT} is the supervised Neural AIDE fine-tuned as in [4]. We compare 4 variations of our FC-AIDE: FC-AID_S is the supervised-only model, FC-AID_{S+FT} is the supervised model fine-tuned as Section 3.2, FC-AID_B is the blindly trained model with σ range of $[0, 50]$, and FC-AID_{B+FT} is FC-AID_B fine-tuned with the correct σ . The stopping epochs for all our FC-AIDE models (both supervised and fine-tuned) were selected from a separate validation set that is composed of 32 natural images.

4.2 Denoising results on the standard dataset

Table 1 and 2 summarize the PSNR results on Set13 and BSD68, respectively. RED and MemNet were only tested for $\sigma = 30, 50$, since they did not have the models for other noise levels. Firstly, we can see that for all noise levels, our FC-AID_{S+FT}, which does both supervised training and adaptive fine-tuning, outperforms all other methods for both sets. Particularly, we observe that the supervised model, FC-AID_S, is slightly worse than RED or MemNet, the current state-of-the-arts in the literature, but the fine-tuning makes the model surpass all of them. Secondly, by observing the performance gap between FC-AID_S and N-AID_S, we can clearly see the benefit of the proposed fully convolutional architecture in Section 3.1. Thirdly, we observe that FC-AID_{B+FT} performs almost as well as FC-AID_{S+FT} and much better than DnCNN-B. This result shows that as long as the correct σ of the given noisy image is known, the blindly trained model alone can compete with and outperform other separately trained matched models via adaptive fine-tuning step.

4.3 Denoising results on the mismatched dataset

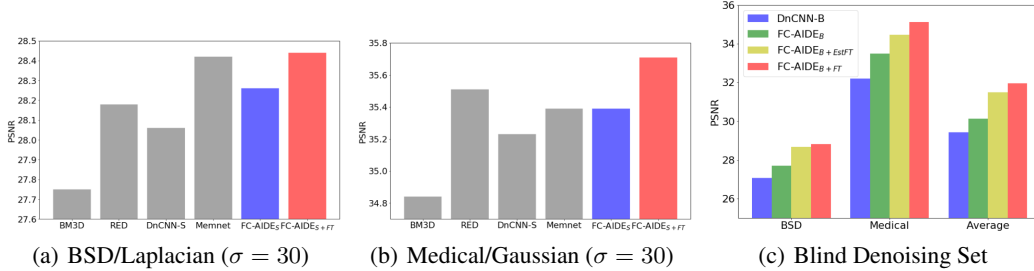


Figure 3: PSNR results on mismatched datasets.

We now compare the performance of FC-AIDE with other methods on the mismatched dataset, BSD/Laplacian and Medical/Gaussian, and Figure 3(a) and Figure 3(b) show the PSNR results. Note all RED, MemNet, DnCNN-S, and FC-AID_S are supervised trained on natural images with Gaussian noise with $\sigma = 30$. Again, we observe that FC-AID_{S+FT} performs the best on both datasets and confirm the power of the adaptive fine-tuning; namely, even when the noise distribution or the image characteristics of the given noisy image is different from what the supervised model is trained for, the fine-tuning can adapt to that difference very well and perform superb denoising. We note MemNet is relatively strong for noise mismatch (*i.e.*, BSD/Laplacian), but is weak for image mismatch (*i.e.*, Medical/Gaussian).

To show another result on image mismatch, Table 15 again shows the PSNR results of the 3 images in Set13, {Barbara, F.print, Einstein}, for $\sigma = 30$. Barbara and F.print are images with regular textures with high self-similarities, and CNN-based denoisers are well-known to suffer for

those images. Einstein is a halftone image that also has radically different characteristics from the natural images. From the table, we indeed observe that the supervised-only CNN-based denoisers, including FC-AIDE_S, perform worse than the non-local filter based BM3D. However, we see that FC-AIDE_{S+FT} gets very close to BM3D for Barbara and much better than all other for F.print and Einstein, again showing the power of the adaptivity it achieves via fine-tuning.

Table 3: PSNR(dB) on the 3 images of Set13 for $\sigma = 30$.

Image	BM3D	RED	Memnet	DnCNN-S	FC-AIDE _S	FC-AIDE _{S+FT}
Barbara	29.79	29.27	29.11	28.93	29.04	29.65
F.print	26.84	26.80	26.63	26.59	26.65	27.17
Einstein	22.64	21.77	21.29	20.54	20.50	23.26

Finally, Figure 3(c) shows the results on the Blind Denoising Set that has various image characteristics, noise distribution, and noise level. The FC-AIDE_{B+EstFT} is our FC-AIDE that fine-tunes the blindly trained FC-AIDE_B with the estimated $\hat{\sigma}$ obtained by the binary search algorithm. Thus, FC-AIDE_{B+EstFT} is the exact same blind model as DnCNN-B and FC-AIDE_B. The figure shows the PSNR results for the natural images (BSD) and medical images in the dataset, and the overall average of them. We can clearly see that FC-AIDE_{B+EstFT} significantly outperforms DnCNN-B, for more than 2dB on average. Moreover, FC-AIDE_{B+EstFT} gets close to FC-AIDE_{B+FT}, which does fine-tuning with the *correct* σ for each image, suggesting that our σ estimation algorithm is accurate enough. In fact, as we report in the Supplementary Material, we perfectly estimate for $\sigma = \{15, 25, 50\}$, and only misses the half of the images with $\sigma = 75$ by estimating with $\hat{\sigma} = 70$. We believe this is a strong result, since blindly estimating the noise σ only from the noisy image is extremely a hard problem.

4.4 Ablation study

Here, we carry out the ablation study for our FC-AIDE. Figure 4(a) shows the average PSNR curves with respect to the training epoch on BSD68 with $\sigma = 25$ and compares our FC-AIDE_S with three other supervised models; Model 1, which only uses the combined feature map of Layer 22 and does not have any 1×1 residual blocks, Model 2, which adds two final 1×1 residual blocks to Model 1, and Model 3, which uses all intermediate feature maps as our FC-AIDE, but does not have the inner 1×1 residual blocks. From the figure, we clearly see the contribution of each architecture block in achieving high PSNR of FC-AIDE. Figure 4(b) shows the average PSNR of FC-AIDE with respect to the fine-tuning epoch on BSD68 and compares the data augmented fine-tuning of Section 3.2 and the original fine-tuning in [4] that only uses the given noisy image \mathbf{Z} without flipping. Again, we clearly see the benefit of the data augmented fine-tuning. Furthermore, we see both PSNR curves are quite robust to the epochs, which validates choosing the stopping epoch with a validation set.

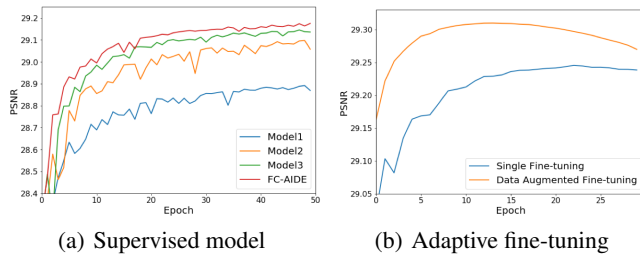


Figure 4: Ablation study for FC-AIDE

5 Conclusion

In this paper, we proposed a novel CNN-based adaptive image denoiser and showed strong empirical results on both standard benchmark dataset and the mismatched datasets. Particularly, the results on the challenging Blind Denoising Set highlights the strong adaptivity of our FC-AIDE algorithm. We believe there are several potential future research directions. First, more sophisticated CNN architectures in [14, 22] can be also used within our QED modules. Moreover, running FC-AIDE in the wavelet domain as in [2] would be also possible since the whiteness of noise is preserved in the wavelet transform and all our tools can carry over. Extending our method to other general estimation problem other than image denoising as in [18] would be another interesting direction to pursue.

6 Supplementary Material

6.1 Proof of Lemma 1

Lemma 2 For any additive noise \mathbf{N} with $\mathbb{E}(\mathbf{N}) = 0$, $\text{Cov}(\mathbf{N}) = \sigma^2 \mathbf{I}$, we have

$$\mathbb{E} \mathbf{L}_n(\mathbf{Z}, \hat{\mathbf{X}}(\mathbf{Z}); \sigma^2) = \mathbb{E} \mathbf{\Lambda}_n(\mathbf{x}, \hat{\mathbf{X}}(\mathbf{Z})). \quad (5)$$

Moreover, when the noise \mathbf{N} is white Gaussian (i.e., AWGN), then, $\mathbf{L}_n(\mathbf{Z}, \hat{\mathbf{X}}(\mathbf{Z}); \sigma^2)$ coincides with the Stein's Unbiased Risk Estimate (SURE)[21].

Proof: We note the expectation of the i -th summand in (Manuscript, Eq.(1)) is

$$\frac{1}{n} \mathbb{E} \left((Z_i - \hat{X}_i(\mathbf{Z}))^2 + \sigma^2 (2a(\mathbf{Z}^{\setminus i}) - 1) \right) \quad (6)$$

$$= \frac{1}{n} \mathbb{E} \left(\mathbb{E} \left((Z_i - \hat{X}_i(\mathbf{Z}))^2 + \sigma^2 (2a(\mathbf{Z}^{\setminus i}) - 1) \mid \mathbf{Z}^{\setminus i} \right) \right) \quad (7)$$

$$= \frac{1}{n} \mathbb{E} \left(\mathbb{E} \left((x_i - \hat{X}_i(\mathbf{Z}))^2 \mid \mathbf{Z}^{\setminus i} \right) \right) = \frac{1}{n} \mathbb{E} \left(x_i - \hat{X}_i(\mathbf{Z}) \right)^2 \quad (8)$$

in which (8) is from the specific form of $\hat{X}_i(\mathbf{Z})$ and the fact that $\mathbb{E}(Z_i \hat{X}_i(\mathbf{Z}) \mid \mathbf{Z}^{\setminus i}) = \mathbb{E}(x_i \hat{X}_i(\mathbf{Z}) + \sigma^2 a(\mathbf{Z}^{\setminus i}) \mid \mathbf{Z}^{\setminus i})$, since Z_i and $a(\mathbf{Z}^{\setminus i})$ are independent due to the whiteness of \mathbf{N} and \mathbf{x} being an individual image. Furthermore, when \mathbf{N} is i.i.d. Gaussian, then the SURE of $\mathbf{\Lambda}_n(\mathbf{x}, \hat{\mathbf{X}}(\mathbf{Z}))$ becomes

$$-\sigma^2 + \frac{1}{n} \|\mathbf{Z} - \hat{\mathbf{X}}(\mathbf{Z})\|_2^2 + \frac{2\sigma^2}{n} \sum_{i=1}^n \frac{\partial \hat{X}_i(\mathbf{Z})}{\partial Z_i}, \quad (9)$$

which is equivalent to (Manuscript, Eq.(1)) when $\hat{X}_i(\mathbf{Z}) = a(\mathbf{Z}^{\setminus i})Z_i + b(\mathbf{Z}^{\setminus i})$. ■

6.2 Supplementary Material for Section 3.3

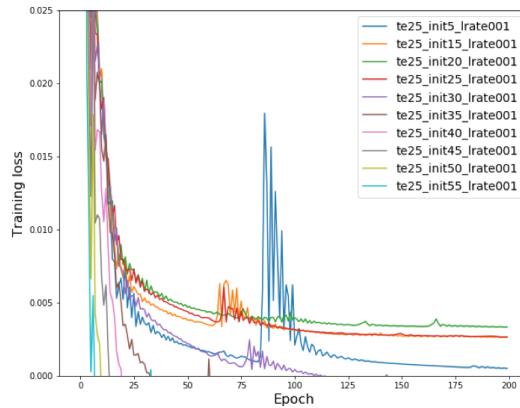


Figure 5: Training curves for fine-tuning with mismatched $\tilde{\sigma}$'s when the true $\sigma = 25$.

Figure 5 exemplifies training loss curves for fine-tuning a randomly initialized FC-AIDE model on a single 512×512 image with several different $\tilde{\sigma}$'s when the true σ was 25. The figure empirically confirms our observation made in Section 3.3; that is, the training loss becomes negative only when fine-tuning with $\tilde{\sigma} > \sigma$ in the estimated loss. The simple binary search algorithm for σ estimation based on this observation is given in Algorithm 1

Algorithm 1 Binary search algorithm for σ estimation

Require: Noisy image \mathbf{Z} , Maximum number of epoch e_{\max} **Ensure:** Estimated noise $\hat{\sigma}$ Set $\Sigma = \{5, 10, \dots, 95, 100\}$, $\sigma_c = 100$, $V = \phi$ **while** Σ **not** ϕ **do**Randomly initialize the neural network parameter \mathbf{w}_0 **for** $t = 1 : e_{\max}$ **do**Update \mathbf{w}_t from \mathbf{w}_{t-1} using (Manuscript, Eq.(4)) and Adam [12] optimizerEvaluate $L = \mathbf{L}_n(\mathbf{Z}, \hat{\mathbf{X}}_{\text{FC-AIDE}}(\mathbf{w}_t, \mathbf{C}_{k \times k}); \sigma_c^2)$ **if** $L \leq 0$ **then break****end for****if** $L \leq 0$ **then** $S = \{\sigma \in \Sigma : \sigma \geq \sigma_c\}$ **else** $S = \{\sigma \in \Sigma : \sigma \leq \sigma_c\}$, $V \leftarrow V \cup \{\sigma_c\}$ **endif**Update $\Sigma \leftarrow \Sigma \setminus S$ and $\sigma_c = \text{median}(\Sigma)$ **end while** $\hat{\sigma} = \max V$

6.3 Experimental results

Table 4: PSNR on Set13 ($\sigma=15$).

PSNR	BM3D	RED	DnCNN-S	DnCNN-B	Memnet	NAIDE _S	NAIDE _{S+FT}	FC-AIDE _S	FC-AIDE _{S+FT}	FC-AIDE _B	FC-AIDE _{B+FT}
Barbara	33.04	-	32.56	32	-	32.29	32.71	32.45	33.05	31.92	32.94
Boat	32.09	-	32.39	32.32	-	32.21	32.4	32.34	32.62	32.25	32.6
Couple	32.11	-	32.45	32.4	-	32.25	32.28	32.43	32.55	32.33	32.53
Fprint	30.27	-	30.37	30.3	-	30.25	30.62	30.35	30.72	30.18	30.7
Hill	31.87	-	32.11	32.01	-	31.95	32.04	32.07	32.24	31.93	32.22
Lena	34.25	-	34.56	34.52	-	34.32	34.41	34.53	34.69	34.45	34.67
Man	31.9	-	32.41	32.35	-	32.19	32.22	32.33	32.44	32.23	32.4
Flintstone	32.99	-	32.71	32.52	-	32.62	33.24	32.78	33.65	32.58	33.6
Cman	31.85	-	32.55	32.03	-	32.25	32.44	32.46	32.69	31.94	32.59
House	34.96	-	35.05	34.98	-	34.81	34.98	35.11	35.47	34.88	35.41
Peppers	32.72	-	33.32	33.22	-	33.11	33.23	33.19	33.4	32.97	33.4
Einstein	26.94	-	26.44	20.54	-	24.63	27.26	25.42	27.58	23.91	27.27
Shannon	30.69	-	31.78	31.4	-	30.1	32.03	31.52	32.58	30.84	32.39
Average	31.98	-	32.21	31.58	-	31.77	32.30	32.08	32.59	31.72	32.52

Table 5: SSIM on Set13 ($\sigma=15$).

SSIM	BM3D	RED	DnCNN-S	DnCNN-B	Memnet	NAIDE _S	NAIDE _{S+FT}	FC-AIDE _S	FC-AIDE _{S+FT}	FC-AIDE _B	FC-AIDE _{B+FT}
Barbara	0.9213	-	0.9192	0.9157	-	0.9095	0.9134	0.9129	0.9197	0.9083	0.9187
Boat	0.8533	-	0.8604	0.8583	-	0.8605	0.8677	0.8651	0.8751	0.862	0.8745
Couple	0.8749	-	0.8818	0.8816	-	0.8808	0.8827	0.8869	0.8906	0.8846	0.8899
Fprint	0.9472	-	0.9511	0.9504	-	0.9595	0.9626	0.9608	0.9634	0.9592	0.9633
Hill	0.8398	-	0.8472	0.8426	-	0.8323	0.8371	0.8386	0.8441	0.8324	0.8436
Lena	0.8957	-	0.8998	0.8993	-	0.8797	0.8819	0.8852	0.8891	0.8835	0.889
Man	0.8663	-	0.88	0.8785	-	0.8563	0.8572	0.8611	0.8649	0.8584	0.8638
Flintstone	0.9294	-	0.9299	0.9284	-	0.9239	0.9279	0.9277	0.9346	0.9264	0.9347
Cman	0.8961	-	0.9134	0.9004	-	0.903	0.9055	0.9092	0.9082	0.8968	0.9082
House	0.8915	-	0.8843	0.885	-	0.8622	0.8668	0.8663	0.8815	0.8642	0.8815
Peppers	0.9088	-	0.9129	0.9121	-	0.9132	0.9141	0.9166	0.9176	0.9149	0.9176
Einstein	0.9789	-	0.9806	0.9434	-	0.9683	0.9823	0.9727	0.9822	0.9632	0.9822
Shannon	0.99	-	0.9915	0.9908	-	0.9841	0.987	0.9878	0.99	0.9847	0.99
Average	0.9072	-	0.9117	0.9067	-	0.9026	0.9066	0.9070	0.9124	0.9030	0.9121

Table 6: PSNR on Set13 ($\sigma=25$).

PSNR	BM3D	RED	DnCNN-S	DnCNN-B	Memnet	NAIDE _S	NAIDE _{S+FT}	FC-AIDE _S	FC-AIDE _{S+FT}	FC-AIDE _B	FC-AIDE _{B+FT}
Barbara	30.61	-	29.92	29.59	-	29.52	29.97	29.93	30.49	29.56	30.37
Boat	29.83	-	30.16	30.14	-	29.95	30.08	30.17	30.4	30.1	30.35
Couple	29.66	-	30.06	30.05	-	29.81	29.84	30.12	30.25	30.01	30.19
Fprint	27.73	-	27.66	27.67	-	27.42	27.93	27.64	28.1	27.5	28.09
Hill	29.8	-	29.98	29.96	-	29.82	29.88	29.99	30.16	29.92	30.1
Lena	32.03	-	32.41	32.4	-	32.14	32.24	32.46	32.65	32.35	32.6
Man	29.55	-	30.05	30.03	-	29.82	29.82	30.01	30.11	29.93	30.07
Flintstone	30.43	-	30.34	30.27	-	30.2	30.73	30.53	31.36	30.42	31.28
Cman	29.4	-	30.1	29.9	-	29.72	29.86	30.06	30.24	29.71	30.13
House	32.82	-	32.97	32.95	-	32.67	32.8	33.16	33.39	32.88	33.2
Peppers	30.16	-	30.82	30.74	-	30.6	30.72	30.76	30.94	30.54	30.9
Shannon	23.83	-	22.59	18.19	-	14.2	23.37	21.58	24.43	20.95	24.08
Einstein	26.89	-	28.07	28	-	26.39	28.43	27.99	29.25	27.53	29.02
Average	29.44	-	29.63	29.22	-	28.64	29.67	29.57	30.14	29.34	30.03

Table 7: SSIM on Set13 ($\sigma=25$).

SSIM	BM3D	RED	DnCNN-S	DnCNN-B	Memnet	NAIDE _S	NAIDE _{S+FT}	FC-AIDE _S	FC-AIDE _{S+FT}	FC-AIDE _B	FC-AIDE _{B+FT}
Barbara	0.8826	-	0.8756	0.8726	-	0.8554	0.8656	0.8695	0.8805	0.8609	0.8773
Boat	0.7995	-	0.8087	0.8094	-	0.8022	0.8079	0.8131	0.8228	0.8104	0.8212
Couple	0.8156	-	0.827	0.8276	-	0.8184	0.8218	0.8327	0.8387	0.8289	0.8367
Fprint	0.9091	-	0.9134	0.9135	-	0.9235	0.9319	0.928	0.9339	0.9257	0.9337
Hill	0.7752	-	0.7799	0.7794	-	0.7553	0.76	0.7655	0.7711	0.7622	0.7689
Lena	0.86	-	0.8684	0.869	-	0.8389	0.8414	0.8506	0.8562	0.8477	0.8549
Man	0.8008	-	0.8197	0.8193	-	0.7792	0.7803	0.7919	0.7961	0.7877	0.7937
Flintstone	0.9021	-	0.9047	0.904	-	0.8944	0.9	0.9043	0.9136	0.9012	0.9125
Cman	0.8473	-	0.8748	0.8648	-	0.8559	0.8593	0.8701	0.8692	0.8559	0.8672
House	0.86	-	0.8587	0.8595	-	0.8291	0.8268	0.8352	0.839	0.8334	0.8357
Peppers	0.8674	-	0.8795	0.8788	-	0.8733	0.8758	0.8814	0.8826	0.8768	0.8812
Einstein	0.9565	-	0.9538	0.8953	-	0.7964	0.9558	0.9384	0.9672	0.9266	0.9643
Shannon	0.9806	-	0.9841	0.9835	-	0.9678	0.9817	0.9799	0.9845	0.9767	0.984
Average	0.8659	-	0.8729	0.8674	-	0.8454	0.8622	0.8662	0.8735	0.8611	0.8716

Table 8: PSNR on Set13 ($\sigma=30$).

PSNR	BM3D	RED	DnCNN-S	DnCNN-B	Memnet	NAIDE _S	NAIDE _{S+FT}	FC-AIDE _S	FC-AIDE _{S+FT}	FC-AIDE _B	FC-AIDE _{B+FT}
Barbara	29.79	29.27	28.93	28.83	29.11	-	-	29.04	29.65	28.75	29.55
Boat	29.07	29.44	29.33	29.36	29.42	-	-	29.4	29.6	29.34	29.55
Couple	28.85	29.36	29.19	29.23	29.39	-	-	29.32	29.44	29.2	29.38
Fprint	26.84	26.8	26.59	26.68	26.63	-	-	26.65	27.17	26.56	27.17
Hill	29.11	29.37	29.25	29.29	29.31	-	-	29.32	29.48	29.26	29.43
Lena	31.24	31.79	31.6	31.63	31.79	-	-	31.7	31.9	31.61	31.85
Man	28.81	29.3	29.22	29.22	29.27	-	-	29.21	29.3	29.13	29.26
Flintstone	29.44	29.63	29.4	29.44	29.58	-	-	29.69	30.39	29.58	30.4
Cman	28.62	29.36	29.25	29.17	29.37	-	-	29.25	29.44	28.91	29.29
House	32.05	32.68	32.32	32.4	32.68	-	-	32.58	32.82	32.35	32.69
Peppers	29.4	30.12	30.01	30.01	30.08	-	-	30	30.19	29.78	30.09
Einstein	22.64	21.77	20.54	17.37	21.29	-	-	20.5	23.26	19.79	22.98
Shannon	25.45	26.93	26.71	26.68	26.88	-	-	26.77	27.95	26.28	27.78
Average	28.56	28.91	28.64	28.41	28.83	-	-	28.73	29.28	28.50	29.19

Table 9: SSIM on Set13 ($\sigma=30$).

SSIM	BM3D	RED	DnCNN-S	DnCNN-B	Memnet	NAIDE _S	NAIDE _{S+FT}	FC-AIDE _S	FC-AIDE _{S+FT}	FC-AIDE _B	FC-AIDE _{B+FT}
Barbara	0.8653	0.858	0.8522	0.8539	0.8598	-	-	0.8469	0.8634	0.8391	0.8598
Boat	0.7761	0.7889	0.783	0.7871	0.789	-	-	0.7902	0.7984	0.7875	0.7965
Couple	0.7913	0.8094	0.8018	0.8052	0.8126	-	-	0.8101	0.8164	0.8058	0.8142
Fprint	0.8918	0.8973	0.893	0.896	0.8968	-	-	0.9117	0.92	0.9096	0.9199
Hill	0.75	0.7579	0.7527	0.7559	0.7547	-	-	0.7374	0.7443	0.735	0.7429
Lena	0.8461	0.8604	0.8549	0.8563	0.8612	-	-	0.8364	0.8427	0.8325	0.8401
Man	0.7765	0.797	0.7927	0.7933	0.7958	-	-	0.7606	0.7653	0.7561	0.7622
Flintstone	0.8874	0.8957	0.8904	0.8905	0.8943	-	-	0.8909	0.902	0.8876	0.9016
Cman	0.8281	0.8615	0.8543	0.8493	0.8608	-	-	0.8517	0.8567	0.8369	0.8501
House	0.8503	0.8567	0.8521	0.8533	0.8548	-	-	0.8268	0.8314	0.8242	0.8287
Peppers	0.8571	0.8737	0.8689	0.8687	0.8726	-	-	0.8715	0.8713	0.8663	0.8667
Einstein	0.9441	0.9464	0.925	0.8687	0.9396	-	-	0.9209	0.9557	0.9038	0.9524
Shannon	0.9741	0.9831	0.9774	0.9789	0.9795	-	-	0.9752	0.9816	0.9715	0.9812
Average	0.8491	0.8605	0.8537	0.8505	0.8593	-	-	0.8485	0.8576	0.8428	0.8551

Table 10: PSNR on Set13 ($\sigma=50$).

PSNR	BM3D	RED	DnCNN-S	DnCNN-B	Memnet	NAIDE _S	NAIDE _{S+FT}	FC-AIDE _S	FC-AIDE _{S+FT}	FC-AIDE _B	FC-AIDE _{B+FT}
Barbara	27.24	26.44	26.21	26.39	26.63	25.56	26.25	26.4	27.05	26.12	26.95
Boat	26.73	27.25	27.15	27.18	27.26	26.9	27.03	27.24	27.42	27.14	27.37
Couple	26.4	26.99	26.84	26.84	27.07	26.47	26.5	26.97	27.09	26.82	26.99
Fprint	24.52	24.31	24.13	24.18	24.28	23.86	24.56	24.18	24.79	24.09	24.76
Hill	27.12	27.46	27.36	27.36	27.48	27.12	27.16	27.45	27.58	27.32	27.5
Lena	28.92	29.48	29.31	29.27	29.59	28.89	29.08	29.43	29.68	29.23	29.6
Man	26.74	27.23	27.16	27.16	27.25	26.88	26.91	27.18	27.27	27.06	27.2
Flintstone	26.68	27.29	27.11	27.15	27.4	26.84	27.15	27.36	27.97	27.2	27.85
Cman	26.17	27.17	27.1	27.12	27.22	26.67	26.79	27.1	27.25	26.91	27.18
House	29.75	30.51	30.17	30.2	30.66	29.63	29.84	30.48	30.65	30.07	30.45
Peppers	26.56	27.22	27.17	27.17	27.33	26.93	27.02	27.18	27.41	26.93	27.35
Einstein	20.5	17.16	16.34	15.71	17.55	16.57	20.58	16.89	20.62	16.77	20.48
Shannon	21.38	23.1	23.18	23.21	23.37	22.19	23.66	23.22	24.56	22.95	24.35
Average	26.05	26.28	26.09	26.07	26.39	25.73	26.35	26.24	26.87	26.05	26.77

Table 11: SSIM on Set13 ($\sigma=50$).

SSIM	BM3D	RED	DnCNN-S	DnCNN-B	Memnet	NAIDE _S	NAIDE _{S+FT}	FC-AIDE _S	FC-AIDE _{S+FT}	FC-AIDE _B	FC-AIDE _{B+FT}
Barbara	0.793	0.7739	0.7702	0.7755	0.7919	0.7189	0.745	0.7639	0.7879	0.7521	0.781
Boat	0.7019	0.7228	0.7167	0.7177	0.7251	0.6991	0.7052	0.7198	0.7287	0.715	0.7257
Couple	0.7026	0.7303	0.7216	0.7215	0.7376	0.6967	0.7022	0.7292	0.7369	0.72	0.7312
Fprint	0.8296	0.832	0.8257	0.8283	0.8375	0.8324	0.8606	0.8496	0.8679	0.8479	0.8664
Hill	0.6727	0.6856	0.6796	0.6792	0.6865	0.635	0.6356	0.6554	0.6621	0.6494	0.6582
Lena	0.7965	0.8153	0.8082	0.8056	0.8209	0.7545	0.764	0.7831	0.7934	0.7708	0.789
Man	0.7008	0.7235	0.7186	0.7168	0.7261	0.6498	0.6554	0.6741	0.6793	0.6651	0.6738
Flintstone	0.8394	0.8583	0.8525	0.8512	0.8604	0.8313	0.8386	0.8518	0.8685	0.8427	0.8647
Cman	0.7765	0.8117	0.8051	0.8041	0.8123	0.7717	0.7742	0.7972	0.7989	0.7859	0.794
House	0.8186	0.8322	0.8252	0.8239	0.8348	0.7738	0.7805	0.8011	0.8008	0.7866	0.7952
Peppers	0.7858	0.8117	0.8053	0.8059	0.8132	0.7859	0.7896	0.8011	0.8052	0.7911	0.8063
Einstein	0.9063	0.8233	0.8016	0.7762	0.8381	0.7888	0.9216	0.8203	0.9181	0.8006	0.9185
Shannon	0.9264	0.9601	0.9534	0.9553	0.9538	0.9384	0.9562	0.9524	0.9667	0.9448	0.9614
Average	0.7885	0.7985	0.7911	0.7893	0.8029	0.7597	0.7791	0.7845	0.8011	0.7748	0.7973

Table 12: PSNR on Set13 ($\sigma=75$).

PSNR	BM3D	RED	DnCNN-S	DnCNN-B	Memnet	NAIDE _S	NAIDE _{S+FT}	FC-AIDE _S	FC-AIDE _{S+FT}	FC-AIDE _B	FC-AIDE _{B+FT}
Barbara	25.13	-	23.61	18.48	-	23.2	23.83	24.13	25.08	21.55	24.86
Boat	25.03	-	25.37	18.3	-	25.09	25.13	25.54	25.68	21.35	25.54
Couple	24.67	-	25	18.31	-	24.63	24.7	25.26	25.44	21.41	25.22
Fprint	22.77	-	21.96	18.31	-	21.79	22.63	22.27	23	20.9	22.98
Hill	25.64	-	25.88	18.57	-	25.64	25.67	26.03	26.14	22.05	26.04
Lena	27.2	-	27.6	18.61	-	27.07	27.21	27.91	28.1	22.3	27.85
Man	25.31	-	25.64	18.39	-	25.37	25.37	25.73	25.79	21.73	25.68
Flintstone	24.39	-	24.92	18.87	-	24.62	24.83	25.24	25.72	21.91	25.55
Cman	24.41	-	25.19	19.12	-	24.78	24.88	25.24	25.36	21.63	25.15
House	27.38	-	27.76	18.58	-	27.15	27.42	28.27	28.55	22.07	28.04
Peppers	24.55	-	25.03	18.59	-	24.81	25.1	25.13	25.48	22.14	25.3
Einstein	18.99	-	14.48	14.56	-	13.92	18.52	14.26	18.61	14.76	19.47
Shannon	18.57	-	19.93	19.64	-	19.21	20.68	20.14	21.66	20.11	21.85
Average	24.16	-	24.03	18.33	-	23.64	24.31	24.24	24.97	21.07	24.89

Table 13: SSIM on Set13 ($\sigma=75$).

SSIM	BM3D	RED	DnCNN-S	DnCNN-B	Memnet	NAIDE _S	NAIDE _{S+FT}	FC-AIDE _S	FC-AIDE _{S+FT}	FC-AIDE _B	FC-AIDE _{B+FT}
Barbara	0.7102	-	0.6515	0.313	-	0.6027	0.6277	0.661	0.7083	0.4613	0.6898
Boat	0.6379	-	0.6506	0.2526	-	0.6232	0.6288	0.6518	0.6599	0.3894	0.6502
Couple	0.6218	-	0.6361	0.2666	-	0.6015	0.6128	0.6481	0.663	0.4055	0.6463
Fprint	0.7661	-	0.7375	0.5806	-	0.7369	0.792	0.7744	0.8108	0.7397	0.8098
Hill	0.6087	-	0.6179	0.2279	-	0.5601	0.5627	0.5861	0.5948	0.3616	0.5851
Lena	0.751	-	0.7672	0.2148	-	0.6968	0.7049	0.7446	0.7572	0.3564	0.7394
Man	0.645	-	0.6603	0.2375	-	0.5775	0.5826	0.6068	0.6143	0.3627	0.6012
Flintstone	0.782	-	0.8006	0.3636	-	0.7734	0.7806	0.8078	0.826	0.4903	0.8136
Cman	0.7304	-	0.761	0.3183	-	0.7199	0.7284	0.7549	0.7376	0.4442	0.7109
House	0.7633	-	0.7766	0.2224	-	0.7087	0.7258	0.7564	0.756	0.3451	0.7258
Peppers	0.7243	-	0.748	0.2915	-	0.7208	0.7283	0.7405	0.7544	0.4888	0.7421
Einstein	0.8683	-	0.6914	0.7015	-	0.5719	0.8774	0.635	0.8747	0.6946	0.8905
Shannon	0.8675	-	0.8918	0.7616	-	0.8913	0.9255	0.8998	0.9419	0.8102	0.9293
Average	0.7290	-	0.7223	0.3655	-	0.6757	0.7137	0.7129	0.7461	0.4884	0.7334

Table 14: Average SSIM on Set13.

σ	BM3D	RED	MemNet	DnCNN-S	DnCNN-B	N-AIDE _S	N-AIDE _{S+FT}	FC-AIDE _S	FC-AIDE _{S+FT}	FC-AIDE _B	FC-AIDE _{B+FT}
15	0.9072	-	-	0.9117	0.9067	0.9026	0.9066	0.9070	0.9124	0.9030	0.9121
25	0.8659	-	-	0.8729	0.8674	0.8454	0.8622	0.8662	0.8735	0.8611	0.8716
30	0.8491	0.8605	0.8593	0.8537	0.8505	-	-	0.8485	0.8576	0.8428	0.8551
50	0.7885	0.7985	0.8029	0.7911	0.7893	0.7597	0.7791	0.7845	0.8011	0.7748	0.7973
75	0.7290	-	-	0.7223	0.3655	0.6757	0.7137	0.7129	0.7461	0.4884	0.7334

Table 15: Average SSIM on BSD68.

σ	BM3D	RED	MemNet	DnCNN-S	DnCNN-B	N-AIDE _S	N-AIDE _{S+FT}	FC-AIDE _S	FC-AIDE _{S+FT}	FC-AIDE _B	FC-AIDE _{B+FT}
15	0.8718	-	-	0.8904	0.8864	0.8812	0.8854	0.8857	0.8903	0.8824	0.8897
25	0.8013	-	-	0.8278	0.8238	0.8099	0.8174	0.8231	0.8281	0.8160	0.8264
30	0.7727	0.8044	0.8035	0.7997	0.7977	-	-	0.7948	0.8013	0.7881	0.7992
50	0.6866	0.7234	0.7291	0.7183	0.7155	0.6832	0.6963	0.7099	0.7181	0.7016	0.7140
75	0.6216	-	-	0.6462	0.3046	0.5977	0.6153	0.6344	0.6464	0.4206	0.6346

Table 16 shows the σ estimation result on the Blind Denoising Set. Each column is for each noise level in the Blind Denoising Set, and each cell shows (number of images with correctly estimated σ) / (total number of images with corresponding noise level, noise distribution, and image characteristics). Note we have perfect estimations for $\sigma = 15, 25, 50$, and miss half of the images with $\sigma = 75$.

Table 16: Results of σ estimation for Blind Denoising Set

		$\sigma=15$	$\sigma=25$	$\sigma=50$	$\sigma=75$
Gaussian	BSD	8 / 8	7 / 7	7 / 7	8 / 8
	Medical	7 / 7	8 / 8	8 / 8	2 / 7
Laplacian	BSD	8 / 8	7 / 7	7 / 7	4 / 8
	Medical	7 / 7	8 / 8	8 / 8	1 / 7

6.4 Visualizations of Set13 and sample medical images



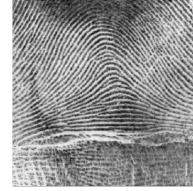
(a) Barbara



(b) Boat



(c) Couple



(d) F.print



(e) Flintstone



(f) Men



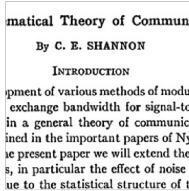
(g) Hill



(h) C.men



(i) Einstein



(j) Shannon



(k) Peppers



(l) House



(m) Lena

Figure 6: Visualization of Set13

The denoising results of several images in Set13 is given at the end of this Supplementary Material.

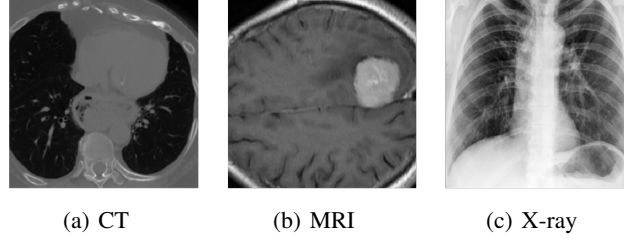


Figure 7: Visualization of sample medical images

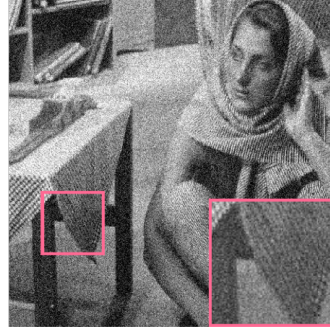
References

- [1] National cancer institute clinical proteomic tumor analysis consortium (cptac). <https://doi.org/10.7937/k9/tcia.2018.oblamn27>.
- [2] W. Bae, J.J. Yoo, and J.C. Ye. Beyond deep residual learning for image restoration: Persistent homology-guided manifold simplification. In *CVPR*, 2017.
- [3] A. Buades, B. Coll, and J. M. Morel. A review of image denoising algorithms, with a new one. *SIAM Journal on Multiscale Modeling and Simulation: A SIAM Interdisciplinary Journal*, 2005.
- [4] Sungmin Cha and Taesup Moon. Neural adaptive image denoiser. *IEEE ICASSP*, 2018.
- [5] Jun Cheng. Brain tumor dataset, 2017.
- [6] K. Dabov, A. Foi, V. Katkovnik, and K. Egiazarian. Image denoising by sparse 3-d transform-domain collaborative filtering. *IEEE Trans. Image Processing*, 16(8):2080–2095, 2007.
- [7] D. Donoho and I. Johnstone. Adapting to unknown smoothness via wavelet shrinkage. *Journal of American Statistical Association*, 90(432):1200–1224, 1995.
- [8] M. Elad and M. Aharon. Image denoising via sparse and redundant representations over learned dictionaries. *IEEE Trans. Image Processing*, 54(12):3736–3745, 2006.
- [9] Y. Eldar. Rethinking biased estimation: Improving maximum likelihood and the Cramer-Rao bound. *Foundations and Trends in Signal Processing*, 1(4):305–449, 2008.
- [10] M. Everingham, L. Van Gool, C. K. I. Williams, J. Winn, and A. Zisserman. The PASCAL Visual Object Classes Challenge 2012 (VOC2012) Results. <http://www.pascal-network.org/challenges/VOC/voc2012/workshop/index.html>.
- [11] S. Gu, L. Zhang, W. Zuo, and X. Feng. Weighted nuclear norm minimization with applications to image denoising. In *Computer Vision and Pattern Recognition (CVPR)*, 2014.
- [12] D. Kingma and J. Ba. Adam: A method for stochastic optimization. In *International Conference on Learning Representations (ICLR)*, 2015.
- [13] J. Mairal, F. Bach, J. Ponce, G. Sapiro, and A. Zisserman. Non-local sparse models for image restoration. In *International Conference on Computer Vision (ICCV)*, 2009.
- [14] X. Mao, C. Shen, and Y-B. Yang. Image restoration using very deep convolutional encoder-decoder networks with symmetric skip connections. *Neural Information Processing Systems (NIPS)*, 2016.
- [15] D. Martin, C. Fowlkes, D. Tal, and J. Malik. A database of human segmented natural images and its application to evaluating segmentation algorithms and measuring ecological statistics. In *International Conference on Computer Vision (ICCV)*, 2001.
- [16] T. Moon, S. Min, B. Lee, and S. Yoon. Neural universal discrete denoiser. In *Neural Information Processing Systems (NIPS)*, 2016.

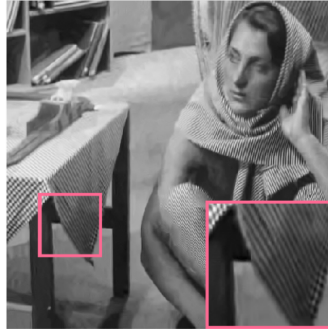
- [17] Giovanni Motta, Erik Ordentlich, Ignacio Ramirez, Gadiel Seroussi, and Marcelo J. Weinberger. The iDUDE framework for grayscale image denoising. *IEEE Trans. Image Processing*, 20:1–21, 2011.
- [18] Y. Romano, M. Elad, and P. Milanfar. Red-ucation: A novel cnn architecture based on denoising nonlinearities. In *ICASSP*, 2018.
- [19] S. Roth and M.J Black. Field of experts. *International Journal of Computer Vision*, 82(2):205–229, 2009.
- [20] K. Sivaramakrishnan and T. Weissman. Universal denoising of discrete-time continuous-amplitude signals. *IEEE Trans. Inform. Theory*, 54(12):5632–5660, 2008.
- [21] C. Stein. Estimation of the mean of a multivariate normal distribution. *The Annals of Statistics*, 9(6):1135–1151, 1981.
- [22] Ying Tai, Jian Yang, Xiaoming Liu, and Chunyan Xu. Memnet: A persistent memory network for image restoration. In *ICCV*, 2017.
- [23] Aäron van den Oord, Nal Kalchbrenner, Oriol Vinyals, Lasse Esleholt, Alex Graves, and Koray Kavukcuoglu. Conditional image generation with PixelCNN decoders. In *NIPS*, 2016.
- [24] Xiaosong Wang, Yifan Peng, Le Lu, Zhiyong Lu, MohammadhadiBagheri, and Ronald M. Summers. Chestx-ray8: Hospital-scale chest x-ray database and benchmarks on weakly-supervised classification and localization of common thorax diseases. In *CVPR*, 2017.
- [25] T. Weissman, E. Ordentlich, G. Seroussi, S. Verdu, and M. Weinberger. Universal discrete denoising: Known channel. *IEEE Trans. Inform. Theory*, 51(1):5–28, 2005.
- [26] K. Zhang, W. Zuo, Y. Chen, D. Meng, and L. Zhang. Beyond a gaussian denoiser: Residual learning of deep cnn for image denoising. *IEEE Trans. Image Processing*, 26(7):3142 – 3155, 2017.



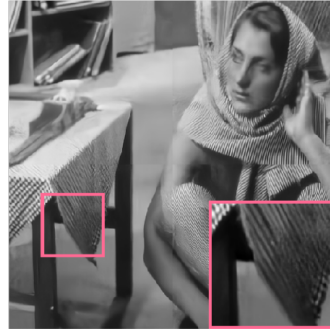
(a) Clean



(b) Noisy($\sigma=30$)



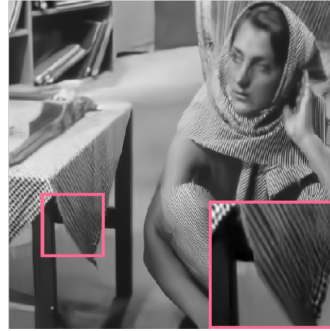
(c) BM3D(PSNR=29.79)



(d) RED(PSNR=29.27)



(e) DnCNN(PSNR=28.93)



(f) Memnet(PSNR=29.11)



(g) FC-AIDE_S(PSNR=29.04)

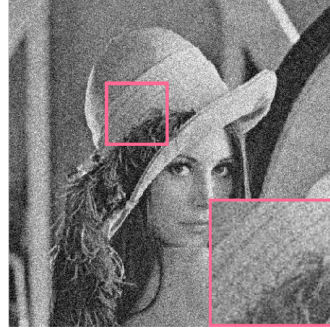


(h) FC-AIDE_{S+FT}(PSNR=29.65)

Figure 8: Denoising results for Barbara



(a) Clean



(b) Noisy($\sigma=30$)



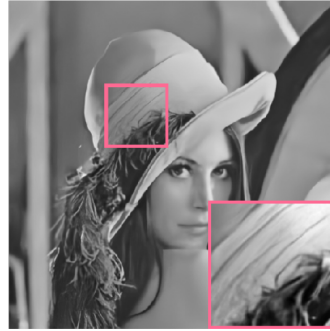
(c) BM3D(PSNR=31.24)



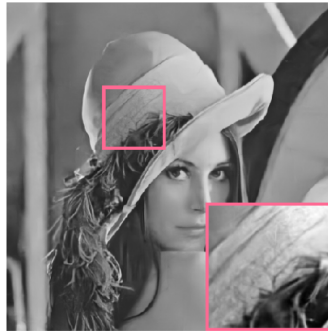
(d) RED(PSNR=31.79)



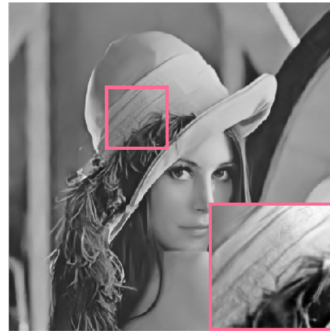
(e) DnCNN(PSNR=31.60)



(f) Memnet(PSNR=31.79)



(g) FC-AIDE_S(PSNR=31.70)

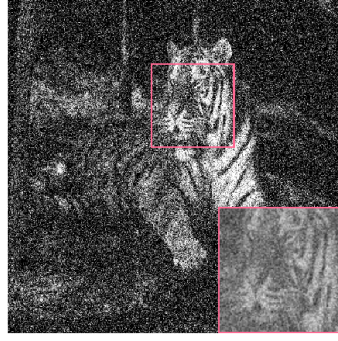


(h) FC-AIDE_{S+FT}(PSNR=31.90)

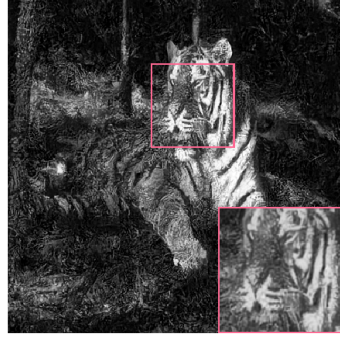
Figure 9: Denoising results for Lena



(a) Clean



(b) Noisy($\sigma=75$)



(c) DnCNN_B(PSNR=20.45)



(d) FC-AIDE_B(PSNR=23.64)

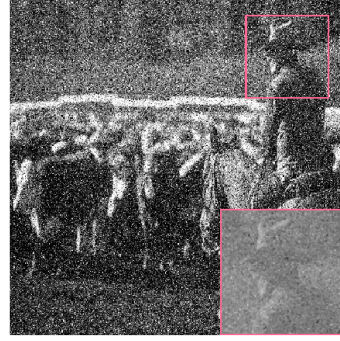


(e) FC-AIDE_{B+EstFT}(PSNR=25.41)

Figure 10: Denoising results for blind test images (Gaussian noise). The noise $\sigma = 75$ is outside the noise levels for which the blind supervised models are trained with.



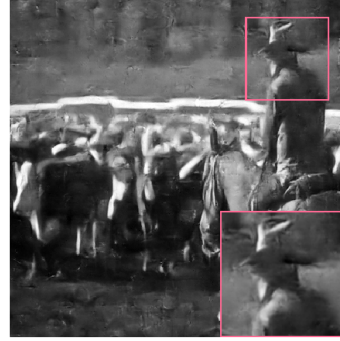
(a) Clean



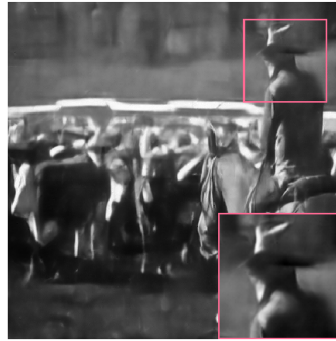
(b) Noisy($\sigma=75$)



(c) DnCNN_B (PSNR=20.33)



(d) FC-AIDE_B (PSNR=22.66)



(e) $\text{FC-AIDE}_{B+EstFT}$ (PSNR=25.26)

Figure 11: Denoising results for blind test images (Laplacian noise). The blind supervised models are trained with Gaussian noise, but the test noise was Laplacian.